Numerical Study of Metal-Oxide Heterojunction Solar Cells

L. Zhu, G. Shao and J. K. Luo*

Institute of Material Research & Innovation, University of Bolton

Deane road, Bolton, BL3 5AB, UK

*corresponding author's email: J.Luo@bolton.ac.uk

Abstract: Metal oxide semiconductors have great potential for photovoltaic (PV) application owing to some optimal bandgaps and variety of possible combinations of the materials. The progress is limited due to lack of high quality materials, reliable process and theoretical study which can guide the development. This paper reports on the numerical modelling of metal oxide semiconductor PV cells. The effects of band gap structure, material, doping concentration and layer thickness on the proposed oxide solar cells have been investigated. It was found that, in an ideal case of no defects and no interface states, wide-gap metal oxide, CuO and Cu_2O can form a heterostructure n/p/p+ junctions with efficiency up to 28.6%, comparable to standard single crystalline solar cells, demonstrating great potential for development.

Keywords: oxide semiconductor, heterojunction, solar cells, TiO_2, CuO, Cu_2O, ZnO/CuO

1. Introduction

Photovoltaic (PV) devices become increasingly important due to energy crisis, limitation in natural fossil fuel resources and associated green-house effect caused by carbon consumption. Si-based solar cells dominate the photovoltaic market owing to the well-established microelectronics industry which provides high quality Si-materials and reliable fabrication processes. However ever-increased demand for photovoltaic devices with better energy conversion efficiency at low cost drives researchers round the world to search for cheaper materials, low-cost processing, and thinner or more efficient device structures. In addition to Si-based solar cells, III-V semiconductor, CuInGaSe and CdS/CdTe-based solar cells, oxide semiconductors such as ZnO- and TiO_2-based dye-sensitized solar cells [1,2] have been developed. Some of them show higher conversion efficiencies than those of Si-cells. However

these photovoltaic devices depend on materials of depleting natural resources which is even worse for the elements such as In and Ga. Elements such as Te, Se and Cd are also potentially toxic. Dye-sensitized solar cells have low conversion efficiency and short lifespan in service due to rapid deterioration of the organic dyes with service time. Amorphous Si based solar cells also suffers from the problem of materials stability.

The search for low cost materials which can be used for better photovoltaic devices is continuing. Metal oxide (MO) semiconductors have received great attention recently owing to the large variety of material types, energy band gaps and structures for PV cells. Pure MO materials are abundant in nature, easy to synthesize and fabricate, therefore they are potential alternative material candidates for PV devices, not even to mention MO semiconductors have many other applications such as transparent conductive oxides [3-5] and photo catalysts [6,7]. For instance, the bandgap of copper oxides (CuO and Cu_2O) are close to the optimal bandgap for PV application, while others such as ZnO and TiO_2 are similar to those of wide bandgap III-V semiconductors, therefore MO semiconductors and combinations of them may provide many choices for the development of low cost solar cells [8-11]

In the past, Cu_2O was successfully used for fabricating solar cells, mostly in Schottky diode format [12-15,18] due to easy synthesis of Cu_2O material and lack of technology for fabrication of p/n junction, and had demonstrated efficiencies up to 1.8% [12]. With the progress in technology, high quality CuO thin films have been achieved. As such CuO has received renewed interests for solar cell application, owing to its optimal bandgap structure, high light absorbance and low thermal emittance [15-17]. Although plenty of choices is available for the absorption layer (A-layer) such as CuO, Cu_2O, NiO_2, MnO_2 etc [15,18,19] and for the window layer (W-layer) such as ZnO, Al-doped ZnO (AZO) and TiO_2 for PV cells, the development of MO solar cells so far has been limited due to lack of high quality materials, reliable processes and most importantly lack of corresponding theoretical study and models which can guide the development of devices with better efficiencies.

The present work is to carry out a theoretical investigation on MO semiconductor based solar cells, in an attempt to identify potential MO-solar cell candidates, to clarify the effects of band gap, band offset etc. on the performance of the devices, and more importantly, to develop the

corresponding solar cell architectures which can be used as a guidance for further practical development. Owing to the large variety of wide band gap materials for the window layer, this work will focus mostly on the heterostructures of wide bandgap MO and CuO/Cu_2O solar cells, and optimize the structure for the best possible performance. The outcome of this work can be extended to other material systems for further exploration.

2. Device structure and modelling methodology

The numerical software AMPS-1D is used for modelling, and the programme solves 1-dimensional dipolar problems according to Poisson's Equation and Continuity Equations. The proposed heterostructure solar cell has a $n^+/p/p^+$ structure as shown in Fig.1(a), as CuO is a natural p-type material. It consists of a wide bandgap window layer (W-layer), an absorption layer (A-layer) and a back layer to enhance the open voltage, V_{OC}, (defined as the V-layer hereafter). For simplicity, the energy band structures for the latter two layers are chosen to be those of pristine CuO and Cu_2O respectively. The bandgaps, E_G, of the three layers are initially set to be ~3.0eV for the window layer, 1.2eV and 2.1eV for the A- and V-layers respectively. To clarify the effect of the V-layer on V_{OC}, a two-layer structure device with the absence of the V-layer is also used in the modelling as shown in Fig.1(b).

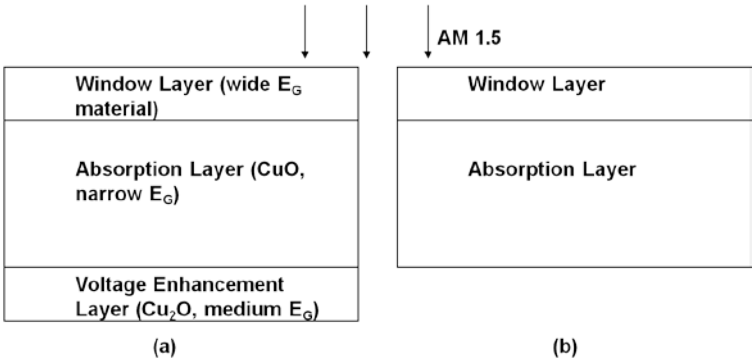

Fig.1 Diagrams of the proposed heterostructure solar cells: (a) Window/Absorber/Voltage enhancer (WAV); (b) Window/Absorber (WA)

To study the hetero-structures effectively, the following assumptions are used for modelling: No negative effects are caused by the contacts, and it gives E_C-E_F=0.1eV for n-type layer, and E_V-E_F=0.1eV for p-type layer at the contacts; the surface recombination speed is set to be $1x10^7$cm/s for both the surfaces and electrodes; only direct band to band recombination was

considered within the semiconductor layers, and the recombination caused by defects (known as SRH recombination) were ignored in the ideal models here; the whole solar spectrum (AM1.5) is absorbed with no reflection from the surface. For simplicity, no interface states for the heterostructures and no defects in conductive layers were considered, i.e. an ideal solar cell. Modelling on MO solar cells with defects and interface states is under progress and will be published subsequently. Other material properties are listed in Tables 1 and 2.

For many direct bandgap MO materials as listed in Table 3, direct band-to-band recombination will be very likely. However, SRH recombination would also happen seriously if deep level traps are introduced by defects. For Auger recombination not considered here, it would not be significant since the carrier densities will not be very high. For indirect MO materials, SRH recombination would dominate. Therefore, the assumptions of the recombination mechanisms in the models may partially show but not the whole picture.

3. Results and discussions

3.1 Two-layer (WA) structure

Before modelling the WAV cell (three-layer structure), it is useful to clarify some effects using the simple two-layer structure (WA-cell). Figure 2a shows the simulated band diagram of a WA cell with a W-layer of 80nm thick and doping concentration of $1x10^{19}cm^{-3}$. The absorption layer is 1500nm thick with a doping concentration of $1x10^{16}cm^{-3}$.

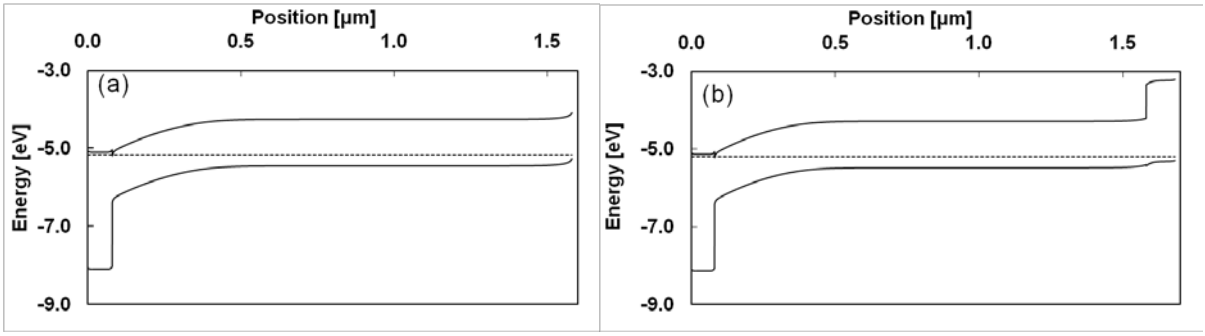

Fig.2 Simulated band diagrams of the WA and WAV solar cells.

Figures 3(a)&(b) show the effect of the thicknesses of the W- and A-layer on the performance of the two-layer structure. The V_{OC} and the fill factor, FF, remain almost unchanged, while the

short circuit current, J_{SC}, and the conversion efficiency, E_{FF}, decrease slowly with the increase of the W-layer thickness from 50nm up to 500nm owing to the absorption of limited short wavelength solar spectrum by the wide bandgap layer (≥400nm for TiO_2). It is obvious that the W-layer should be chosen as thin as possible to achieve good performances. Practically, however, a too thin W-layer (such as 30nm) may show very high sheet resistance if further finger-electrodes are applied, and also may cause short-circuit problems in fabrication due to restrict requirement for clean environments. In addition, the thickness of W-layer cannot affect the performances significantly. Therefore, 80nm for W-layer is considered an optimum thickness for the following solar cell simulations.

Unlike the W-layer thickness, the A-layer thickness has pronounced effect on all performance parameters as shown in Fig.3(b). Particularly, J_{SC} and E_{FF} increase rapidly from 18 to 31mA/cm^2 and from 8.5 to 17.0%, respectively, when the A-layer thickness increases from 250 to 3000nm as a thicker A-layer can absorb more incident solar spectrum for free carrier generation. The A-layer thickness in this MO cell is much thinner than that of single or polycrystalline Si-solar cells owing to the high absorption coefficient of CuO, which is bigger than 1x10^{4}cm^{-1} [15]. Because a 3000nm A-layer gives only about 1% increase in total 16% E_{FF} than a 1500nm A-layer, it might not be worthy fabricating the A-layer with double thickness. Therefore, an optimal A-layer thickness is set to be 1500nm.

It is generally known that the doping concentration in each layer will have a significant effect on the performance of a PV cell. However simulation shows that this is only true for low doping concentration, less than 10^{17}cm^{-3}, in the W layer, and generally low concentration is avoided for the W-layer to minimize the high series resistance. It was found that doping concentration has a limited effect on the cell performance; J_{SC} changes slightly from 29.21 to 29.01mA/cm^2 (less than 1%), while V_{OC} and FF remain almost unchanged as the concentration changes from 1x10^{17}cm^{-3} to 1x10^{20}cm^{-3}, ~~mostly due to the omission of the series resistance in the simulation~~ mostly due to the ignorable further band shift at heavy doping level. To be realistic for low series resistance and good Ohmic contact, a doping concentration of 1x10^{19}cm^{-3} is chosen as the optimal doping for the W-layer in the following simulations.

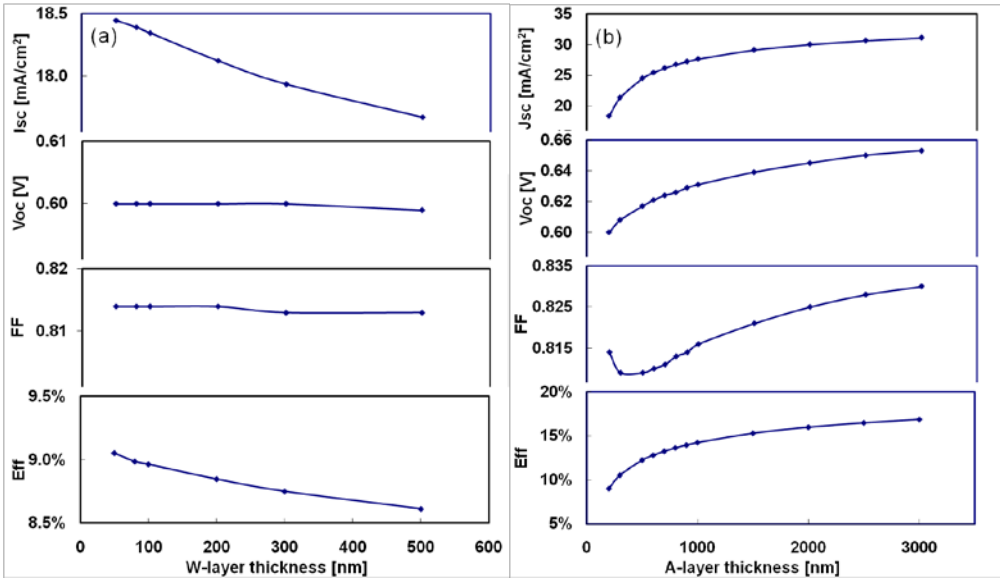

Fig.3 The effects of W-layer (a) and A-layer (b) thickness on the performances of the two-layer cell.

The doping concentration of the A layer shows a much stronger effect on the performance as shown in Fig.4. For doping level up to $5x10^{15}$ cm^{-3}, all the performance parameters remain almost constant. J_{SC} decreases while V_{OC} increases monotonically with doping concentration increase after $1x10^{15}cm^{-3}$. Combination of all the effects leads to a V-shape change of the efficiency against the doping level of the A-layer. At low doping, the depletion region in the A-layer extends to a much larger thickness, which is effective for the generated photo carriers to drift to the terminals. With the increase of the A-layer concentration, the depletion region shrinks, leading to a reduced collection rate of the generated carriers (reduced J_{SC}) for energy conversion. However, the doping concentration has an opposite effect on V_{OC} due to increased band shift against the Fermi-levels in n and p-regions as shown in Fig.5. Since there is a risk of tunnelling leakage for a heavily doped n/p junction, a high concentration A-layer should be avoided. Also V_{OC} can be enhanced by adding a V-layer by the back surface field (BSF) effect as will be discussed later, a doping level of $1x10^{16}cm^{-3}$ is, therefore, set to be the optimal value for the cells. With these optimized parameters, it is found that the two-layer cell could have a conversion efficiency E_{FF} up to 15.76%; with J_{SC} ~ 30.97mA/cm^2, V_{OC}~ 0.62V and FF~0.82. For comparison purpose, Si-cell simulation study by using the software under the same assumptions were done: For a simple two-layered Si-cell similar to Fig 1b, the optimised setting is a top 250nm p-type layer with $1e20cm^{-3}$ doping concentration, covering a bottom

400μm n-type layer with 5e16cm^{-3} doping concentration, which gives an E_{FF}~ 17.64% conversion efficiency, with J_{SC}~ 29.84mA/cm^2 and V_{OC}~ 0.70V [20]. Owing to the massive amount of research and advanced processing technologies, silicon based solar cells can now be made into more complex structures with few defects and interfaces, and obtain a conversion efficiency up to 24.7% [21], very close to the maximum theoretical efficiency 28.8% [22]. Therefore, MO may also have great potential for PV application if sufficient study could be done.

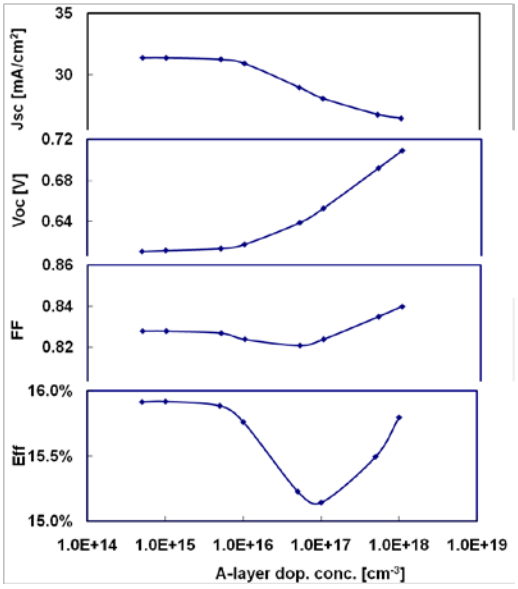

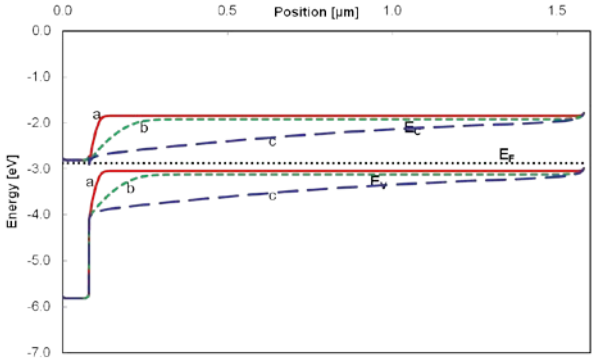

Fig.4 (left) Effects of the A-layer doping concentration on the performances.
Fig.5 (right) Band diagrams for different A-layer doping levels: Curve (a) 1x10^{18} cm^{-3}; (b) 5x10^{16} cm^{-3}; (c) 5x10^{14} cm^{-3}with a constant W-layer doping conc. at 1x10^{19} cm^{-3}.

3.2 Three-layer (WAV) structure

To enhance the V_{OC} and efficiency of the WA structure, a wide-bandgap V-layer is then introduced to form the three layer WAV structure. The pristine p-type Cu_2O is taken as the representative for the simulations though other material systems can be used as well. The parameters for the W- and A-layers are the same as those used in the two-layer structure, while the parameters for the V-layer are to be optimized in the following section. According to the optimised results discussed later, the WAV cell (with 1.2eV A-layer) gives a performance of: J_{SC}~31.48mA/cm^2, V_{OC}~1.03V, FF~0.82 and E_{FF}~26.82%. The conversion efficiency increases by more than 70% comparing to that of the WA structure, mostly owing to the increase of V_{OC} by more than 70%. The band diagram is shown in Fig.2b.

Modelling shows that the thickness of the V-layer has limited effect on the three-layer structure. It is generally believed to be due to the complete absorption by 1500nm A-layer. However detailed study showed even when the A-layer is 100nm, the V-layer thickness has little effect on the performance, i.e. light absorption in V-layer does not contribute to carrier generation. 100nm is then selected for the V-layer hereafter.

3.2.1 V-layer BSF effect and mechanisms

Theoretically, open circuit voltage and short circuit current for a homojunction solar cell cannot be very high simultaneously. Band-gap grading and back surface field (BSF) heterostructure solar cells have been designed and studied to improve V_{OC} without sacrificing J_{SC} significantly [23- 29], but mostly limited to homojunction cells using doping modification, with limited effort for BSF using wide gap layers. Since the V layer is believed to have a similar function to that of a heavily doped BSF layer in Si solar cells [27,30] to enhance the V_{OC}, and a significant BSF effect is expected for MO heterostructure PV cells owing to the large bandgap offset as summarized in Table 3.

The function of the V-layer is to block and reflect the minority carriers to increase the potential for carrier accumulations (Φ_{Accum}) and to reduce the recombination at the back terminal which is strongly affected by the thickness of the A-layer. The effect is studied firstly by varying the A-layer thickness in the range from zero to 3000nm. As shown in Fig.6, V_{OC} is around 1.6V when there is no A-layer, i.e. the W/V single heterojunction structure. But the efficiency η is very low due to limited absorption of solar spectrum by this two layer structure. Introduction of the A-layer with a thickness of 20nm leads to a drastic reduction of V_{OC} from 1.6 to ~1.2V. The rate for V_{OC} reduction drops as the thickness increases, with V_{OC} saturating at ~1V. This shows that the V_{OC} enhancement is caused mainly by the wide-bandgap-induced increase of Φ_{Accum} to compensate for insufficient carrier generation. The results show that a strong V_{OC} enhancement occurs when the V-layer is close to the p-n junction as will be discussed later. However, reduction in the A-layer thickness leads to a reduction of J_{SC}, hence the efficiency. Introduction of the V-layer improves V_{OC} significantly and effectively from ~0.62V to >1V regardless the thickness of the V-layer. But it is clear from the figure that a thickness up to 1500nm for the A-layer is sufficient for absorbing most

of the solar spectrum. It is worthy mentioning that V_{OC}~1.2V approaches E_g/q of the A-layer, the theoretical maximum voltage that can be obtained from the three layer structure. The fact that V_{OC} of the WAV cell is close to the theoretical value, clearly shows that a WAV structure works better than a WA structure does, because of the wider bandgap of the V-layer with respect to that of the A-layer.

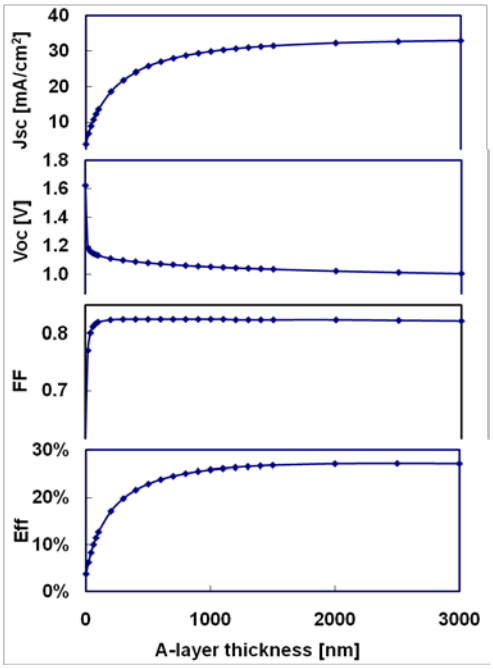

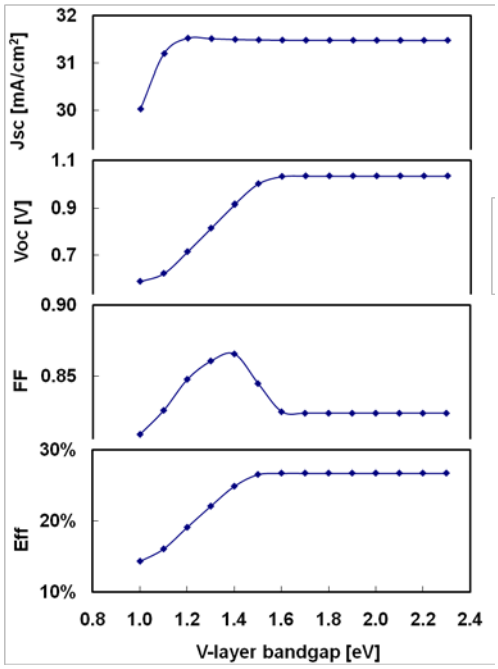

Fig.6 The performance vs. A-layer thickness in the WAV structure (left).
Fig.7 The effect of V-layer bandgap on the performance (right).

Further study is made to clarify the effect of the V-layer bandgap. For simplicity, it is assumed $\Delta E_V \approx 0$ for all the cases, with all the electron affinity values of the V-layer modified correspondingly. The results are summarized in Fig.7. It shows that V_{OC} increases with the bandgap of the V-layer up to E_G=1.6eV, beyond which it saturates. E_G=1.6eV seems to be a critical value, E_{GC}, for the voltage enhancement effect corresponding to $\Delta E_C \approx$0.4eV between the A-layer and V-layer. For $E_G < E_{GC}$, the increased ΔE_C improves the ability of the V-layer to block and reflect the minority carriers; For $E_G > E_{GC}$, however, further increase in ΔE_C is more than the possible maximum kinetic energy of minority carriers, so that no further V_{OC} enhancement can be seen.

The doping concentration of the V-layer has a significant effect on the V_{OC} enhancement, as it modifies the band bending and barrier height as understood from the BSF effect of single crystalline Si-cells [26,30]. The simulated results are shown in Fig.8(a). No effect can be seen

at $E_G > E_{GC}$ as the conduction bandgap offset, $\Delta E > 0.4$eV, alone is sufficient to have the BSF effect. Further increase in barrier height makes no additional contribution. For $E_G < E_{GC}$, it is apparent that V_{OC} increases with the doping concentration of the V-layer. A cell with a $1x10^{19}cm^{-3}$ doped V-layer has a V_{OC} approximately 0.2V larger than that of a $1x10^{16}cm^{-3}$ doped one.

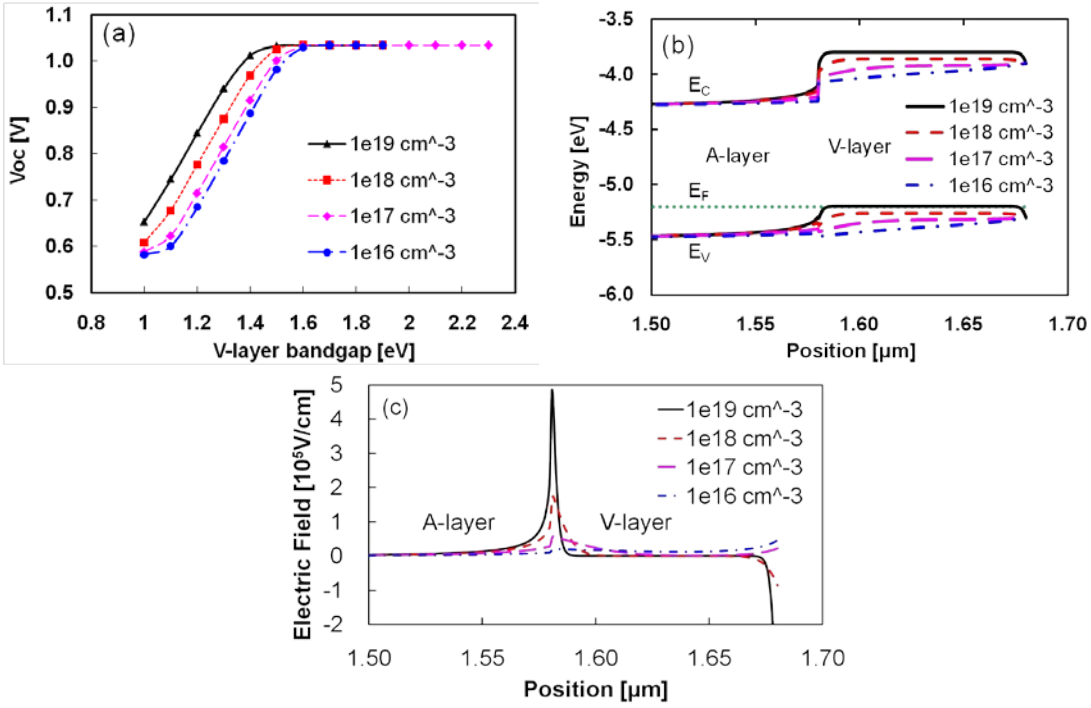

Fig.8 (a) V_{OC} vs. V-layer bandgap for various V-layer doping levels (cm^{-3}); (b) band structures at A/V interface when E_G=1.4eV (<E_{GC}); (c) electric field at A/V interface when E_G = 1.4eV.

Figure 8(b) and (c) illustrate the band diagram and electric field as a function of doping level with E_G fixed at 1.4eV for the V-layer. High concentration in the V-layer has a much more radical change in the band structure and builds up a steeper edge than those with lower doping levels. The steep edge, acting as a 'cliff', is effective in blocking and reflecting the minority carriers, leading to an increased V_{OC}. The results demonstrate two possible methods to enhance V_{OC} and efficiency in MO-structures: introduction of a wide bandgap V-layer and heavy doping for the V-layer. It is interesting to note that the critical E_{GC} value varies as the A-layer thickness changes while all other parameters are fixed as shown in Fig.9. The E_{GC} value is about 1.75eV for a 200nm A-layer, 1.63eV for 500nm, 1.61eV for 1000nm and 1.60eV for 1500nm A-layer respectively. The results imply that a wider bandgap V-layer is

needed for a thinner A-layer cell structure. The reason is as follows: under illumination, some of the free electrons generated in the A-layer will diffuse against the built-in electric field in the depletion region towards the back terminal. They will experience another built-in electric field as a potential barrier at the A/V layer interface. When the p/n junction is close to the V-layer, more free electrons will diffuse and reach the A/V layer interface. Therefore, a higher barrier is required to block and reflect the carriers thoroughly. A wider bandgap V-layer (high E_{GC}) is therefore needed to maximise V_{OC}.

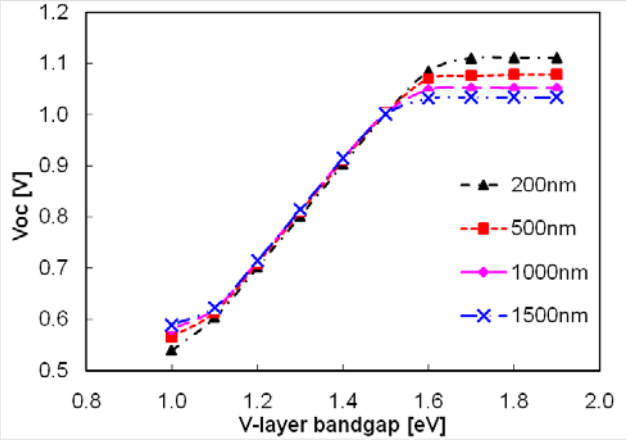

Fig.9 V_{OC} vs. V-layer band gap for various A-layer thicknesses (same settings as in Fig.8).

3.2.2 A-layer bandgap optimisation

As it was clear that the band gap of the A-layer affects J_{SC} in the two-layer cell and V_{OC} in the three-layer cell, it would be useful to further clarify the effect of the A-layer band gap on cell performances. The performances as a function of the A-layer bandgap are illustrated in Fig.10(a) and (b) for the two and three layer cells respectively. The two cell structures show a similar trend of performance against the bandgap of the absorption layer. J_{SC} decreases as the bandgap increases, while V_{OC} and FF rise monotonically. The larger the A layer bandgap, the less solar spectrum can be absorbed, leading to less carriers generated and lower J_{SC}. On the other hand, a cell with a wide A-layer bandgap has a large V_{OC}. As a consequence, the optimal bandgap for the A-layer is around 1.4eV for both the structures as shown in Fig.10, matches well with the optimised value in Ref. [31,32]. With this optimal bandgap value, the possible maximum conversion efficiencies are 19.24% and 28.57% for the two- and three-layer cells respectively, higher than those of 15.76% and 26.82% of the two cells when a 1.2eV A-layer

was used. The optimal three-layer MO cell shows good performance: J_{SC}~27.65mA/cm^2, V_{OC}~1.22V, FF~0.84 and E_{FF}~28.57%.

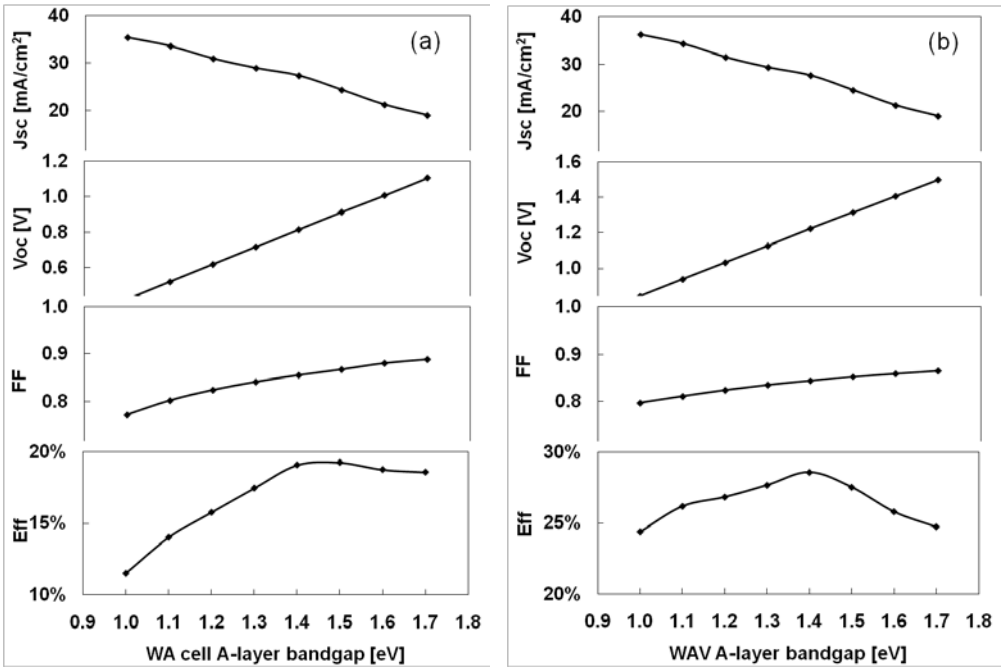

Fig.10 WA (a) and WAV (b) cell performances vs. absorber A-layer bandgap.

CuO was assumed to be the absorption layer for both the structures in the simulation. The reported bandgap of CuO synthesized by various techniques is in the range of 1.2~2.6eV [41-43] and can be controlled using different synthesis conditions. From the simulation results, it is understood that a CuO layer with a bandgap of 1.4eV would be the optimal choice for the fabrication of high efficiency MO solar cells.

3.3 Band offset of the W/A interface (Two-layer structure)

Figure 11 shows the effect of the conduction band offset ΔE_C (the affinity, χ_e, of the A-layer minus χ_e of the W-layer) on the performance of the two layer structure solar cell. Figure 12 shows the extreme cases of the band structures of the cells with different band offsets. It was found that within the range of -0.7~+0.4eV, the band offset has nearly no effect on the performance of the solar cell. When ΔE_C is set beyond that range, FF drops rapidly, leading to deterioration of the efficiency, though Jsc and Voc remain almost unchanged up to ΔE_C=-0.8eV. On the other hand, at $\Delta E_C < 0$, there exists a spiking barrier at the W/A interface

which will block electron transportation towards the front terminal. The results demonstrates that when no SRH recombination caused by defects is considered, this barrier causes no harm to transportation of free carriers, if it is approximately smaller than 2/3 of the A-layer bandgap. When the height of the spiking barrier becomes comparable to the Eg of the A-layer, the minority carriers generated in the A-layer will be stopped from flowing to the front terminal, leading to a drastic reduction of the cell performance. This corresponds to the sharp decline of J_{SC} shown in Fig.11 at ΔE_C = -0.9eV.

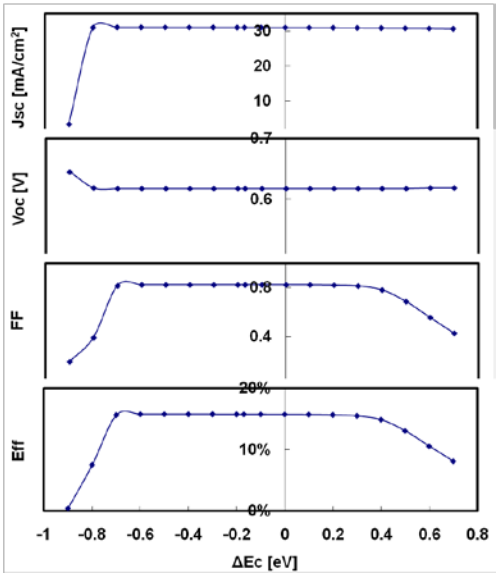

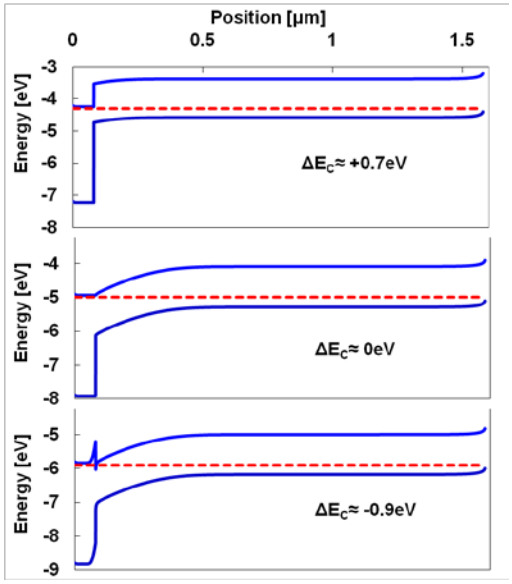

Fig.11 Results of band offset (E_{CA}-E_{CW}=-0.9eV~+0.7eV) simulation (left).

Fig.12 Band structures for various conduction band offset, ΔE_C, within WA structure (right).

4. Heterojunction MO cell materials selection and structure design

According to the simulation, both the WA cell and WAV cell have some advantages respectively. A WA cell has low V_{OC}, but it has only one heterojunction. Therefore it is easier to fabricate and to control the interface states in practice. On the other hand, the WAV structure has high V_{OC} and efficiency, though an additional layer is needed. In practice, an additional interface may introduce more interface states, leading to severe deterioration of the performance. The following are suggestions for metal oxide semiconductor-based solar cells as a general guidance:

1) For the window layer, a wide bandgap, n-type material with high concentration is desirable,

because most MO materials suitable and available for the A-layer fabrication nowadays are natural p-type materials with low doping concentrations.

2) A narrow bandgap material with a low doping concentration can be fabricated a good absorption layer to raise carrier generation rate. However, the bandgap should not be too narrow as low E_G sacrifices V_{OC} significantly. If a BSF V-layer structure is used, then material with slightly small E_G for A-layer could be selected, as V_{OC} can be compensated by the BSF effect.

3) A wide bandgap material should be selected as the BSF V-layer to enhance V_{OC} and efficiency. If the bandgap of the material is not large enough ($<E_{GC}$), then it can be improved by heavily doping in this layer.

4) The material combination for the W-layer and A-layer should be considered carefully. The conduction band offset between the W- and A-layer (p/n junction) will form a barrier for the transportation of the minority carriers, leading to deteriorated performance. In principle, the affinity difference of the two materials should not be greater than 2/3 of the bandgap of the A-layer.

From the structure design point of view, the following issues should be considered: 1) the W-layer can be fabricated very thin because it is not the main absorption layer. and it is desirable for it to be heavily doped to offer a wide depletion region in the A-layer; 2) The A-layer can be designed thick enough to absorb most of the solar spectrum, but not too thick as it will reduce the BSF effect, if applicable. 3) a heavily doped thin V-layer is desirable.

As shown in Table 3, it is understood that materials with wide E_G (>2eV) such as ZnO, ITO, TiO_2, GaP and GaN can be selected for the W- and V-layer fabrication, while materials with narrow E_G (1.0eV~1.5eV) such as CuO, Si and GaAs can be used for the A-layer. The electron affinity χ_e of the W- and A-layer materials should be about the same, or at least $<2/3E_G$ of the A-layer, which makes ΔE_C small enough to prevent the introduction of a potential barrier at the A/V interface. For the WAV cell, the value of $E_G + \chi_e$ of the materials for the A- and V-layers should have similar values to minimize the valence band offset. Since the χ_e of narrow bandgap A-layer materials are mostly around 4eV, the materials suitable for

the W-layer should also have χ_e around 4eV; because the (χ_e+E_G) for A-layer materials are about 5.2~5.7eV, the materials suitable for V-layer fabrication should also have (χ_e+E_G) about 5.2~5.7eV. For example, ZnO, TiO_2 – CuO, Si, GaAs might be the candidate materials for WA cells, while ZnO, TiO_2 – CuO, Si – Cu_2O, AlP, and ZnO, TiO_2 –GaAs – GaP for WAV cells.

5. Conclusions

The feasibility of metal oxide materials for PV solar cell application has been studied by numerical simulation. The effect of doping concentration, layer thickness and band gap structure on oxide semiconductor solar cells have been investigated in detail and the corresponding mechanisms are discussed. It is possible to fabricate PV cells with efficiency up to 19%, by the coupling of a wide band gap oxide with a narrow gap oxide. The efficiency of oxide solar cells can be further enhanced using a wide gap oxide as a BSF layer. For an ideal case without considering defects and interface states, metal oxide semiconductor heterostructures such as TiO_2/CuO/Cu_2O could show a theoretical efficiency of 28.6%, which demonstrates great potential for investment and development.

Acknowledgements: The authors would like to acknowledge the financial support from the Technology Strategy Board under the grant No. TP11/LCE/6/I/AE142J.

Table 1 Simulation parameters for each layer

	W (n+)	A (p)	V (WAV) (p)
Thickness (nm)	80	1500	100
Acceptor concentration (cm-3)	0	$1.0x10^{16}$	$1.0x10^{17}$
Donor concentration (cm-3)	$1.0x10^{19}$	0	0
Band gap (eV)	3.0	1.2	2.1
Electron affinity (eV)	3.9	4.07	3.2
Relative permittivity	86	18.1	9
Hole mobility (cm2/V-s)	20	10	40
Electron mobility (cm2/V-s)	10	0.1	20
Effective density of states-cond. band (cm^{-3})	$1.32x10^{20}$	$3.0x10^{19}$	$2.02x10^{18}$
Effective density of states-vala. band (cm^{-3})	$1.50x10^{21}$	$5.54x10^{20}$	$1.11x10^{19}$
Absorption coefficient (cm^{-1})*	$5x10^{4}$	$1x10^{4}$~$5x10^{5}$	$5x10^{3}$~$5x10^{5}$

Note: Absorption coefficient (cm^{-1}) is not a fixed value but varies with wave length. The table shows a range.

Table 2 Variable setting ranges and the corresponding constant settings. (Parameters in the brackets are in the sequence of W- thickness, A- thickness, W- doping conc. and A- doping conc.)

	1st layer (W) thickness	2nd layer (A) thickness	1st layer doping conc.	2nd layer doping conc.
Variables	50~500nm	200~3000nm	$1x10^{17}$~$5x10^{19}$ cm^{-3}	$1x10^{15}$~$1x10^{18}$ cm^{-3}
Constants	(--,200,$1x10^{18}$,$5x10^{16}$)	(80,--,$1x10^{18}$,$5x10^{16}$)	(80,1500,--,$5x10^{16}$)	(80,1500,$1x10^{19}$,--)

Table 3 Bandgap and electron affinity of common MO materials and semiconductors.

Materials	E_G (eV)	Xe (eV)	E_G + Xe (eV)	Ref.
ZnO	3.40	4.2~4.6	7.6~8	[33-35]
TiO_2	3.0~3.3	3.9~4.1	6.9~7.4	[36-38]
ITO	3.6~4.06	>4.7(work function)	8.3~8.76	[34,39,40]
GaN	3.20	3.30	6.50	[33]
CuO	1.21~1.51	4.07	5.28~5.58	[41-43]
Si	1.12	4.05	5.17	[33]
GaAs	1.45	4.15	5.60	[33]
InP	1.34	4.40	5.74	[33]
Cu_2O	2.10	3.20	5.30	[34,38,44]
Fe_2O_3	2.0~2.1	3.88	5.88~5.98	[45,46]
AlP	2.56	2.80	5.36	[33]
GaP	2.25	3.20	5.45	[33]

References

[1] P. Raksa, S. Nilphai, A. Gardchareon and S. Choopun, Copper Oxide Thin Film and Nanowire as a Barrier in ZnO Dye-sensitized Solar Cells, *Thin Solid Films*, Vol.517, pp.4741-4744, 2009

[2] S. Anandan, Recent Improvements and Arising Challenges in Dye-sensitized Solar Cells, *SolarEnergy Materials and Solar Cells*, Vol.91, pp.843-846, 2007

[3] Y. Sato, H. Akizuki, T. Kamiyama and Y. Shigesato, Transparent Conductive Nb-doped TiO_2 Films Deposited by Direct Current Magnetron Sputtering using a TiO_{2-x} Target, *Thin Solid Films*, Vol.516, pp.5758-5762, 2008

[4] W. Lin, R. Ma, Wei. Shao, Bo. Kang and Z. Wu, Properties of doped ZnO Transparent Conductive Thin Films Deposited by RF Magnetron Sputtering using a Series of High Quality Ceramic Targets, *Rare Materials*, Vol.27, pp.32-35, 2008

[5] Z. Li and D. Ren, Preparation of ITO Transparent Conductive Film by Sol-Gel Method, *Transactions of Nonferrous Metals Society of China*, Vol.16, pp.1358-1361, 2006

[6] C. Xu, L. Cao, G. Su, W. Liu, H. Liu, Y. Yu and X. Qu, Preparation of ZnO/Cu_2O Compound Photocatalyst and Application in Treating Organic Dyes, *Journal of Hazardous Materials*, Vol.176, pp.807-813, 2010

[7] L. Zhang, T. Kanki, N. Sano and A. Toyoda, Development of TiO_2 Photocatalyst Reaction for Water Purification, *Separation and Purification Technology*, Vol.31, pp.105-110, 2003

[8] 1. J. Herion, E.A. Niekisch and G. Scharl, Investigation of Metal Oxide/Cuprous Oxide Heterojunction Solar, *Solar Energy Materials*, Vol.4, pp.101-112, 1980

[9] K. Akimoto, S. Ishizukaa, M. Yanagitaa, Y. Nawaa, Goutam K. Paula and T. Sakurai, Thin Film Deposition of Cu_2O and Application for Solar Cells, *Solar Energy*, Vol.80, pp.715-722, 2006

[10] Z. Duan, N. Pereira, Y. Lu and A. Pasquier, Gel Probe Photocurrent Measurement of Cuprous Oxide Films, *Solar Energy Materials and Solar Cells*, Vol.94, pp.1741-1746, 2010

[11] P. Samarasekara, M.A.K. Mallika Arachchi, A.S. Abeydeera, C.A.N. Fernando, A.S. Disanayake and R.M.G. Rajapakse, Photocurrent Enhancement of DC Sputtered Copper Oxide Thin Films, *Bulletin of Materials Science*, Vol.28-5, pp.483-486, 2005

[12] L.C. Olsen, F.W. Addis and W. Miller, Experimental and Theoretical Studies of Cu_2O Solar Cells, *Solar Cells*, Vol.7, pp.247-279, 1982

[13] B.P. Rai, Cu_2O Solar Cells: A Review, *Solar Cells*, Vol.25, pp.265-272, 1988

[14] S.S. Jeong, A. Mittiga, E. Salza, A. Masci, S. Passerini, Electrodeposited ZnO/Cu_2O Heterojunction Solar Cells, *Electrochimica Acta*, Vol.53, pp.2226-2231, 2008

[15] Ibrahim Y. Erdogan, O. Gullu, Optical and Structural Properties of CuO Nanofilm: Its Diode Application,

Journal of Alloys and Compounds, *Journal of Alloys and Compounds*, Vol.492, pp.378-383, 2010

[16] T. Maruyama, Copper Oxide Thin Films Prepared by Chemical Vapour Deposition from Copper Dipivaloylmethanate, *Solar Energy Materials and Solar Cells*, Vol.56, pp.85-92, 1998

[17] A. Chen, G. Yang, H. Long, F. Li, Y. Li and P. Lu, Nonlinear Optical Properties of Laser Deposited CuO Thin Films, Thin Solid Films, Vol.517, pp.4277-4280, 2009

[18] A.Y. Oral, E. Mensur, M.H. Aslan, E. Basaran, The Preparation of Copper (II) Oxide Thin Films and the Study of Their Microstructures and Optical Properties, *Materials Chemistry and Physics*, Vol.83, pp.140-144, 2004

[19] K. Han, M. Tao, Electrochemically Deposited p-n Homojunction Cuprous Oxide Solar Cells, *Solar Energy Materials & Solar Cells*, Vol.93, pp.153-157, 2009

[20] Detailed simulation inputs and results for Si-cell optimisation under similar assumptions in the software can be obtained on require.

[21] J. Zhao, A. Wang and M.A. Green, High-efficiency PERL andPERT Silicon Solar Cells on FZ and MCZ Substrates, *Solar Energy Materials and Solar Cells*, Vol.65, pp.429-435, 2001

[22] T.M. Razykov, C.S. Ferekides, D. Morel, E. Stefanakos, H.S. Ullal and H.M. Upadhyaya, Solar Photovoltaic Electricity: Current Status and Future Prospects, *Solar Energy*, doi:10.1016/j.solener.2010.12.002

[23] J. Song, S. Li, C.H. Huang, O.D. Crisalle, T.A. Anderson, Device Modelling and Simulation of the Performance of $Cu(In_{1-x},Ga_x)Se_2$ Solar Cells, *Solid –State Electronics*, Vol.48, pp.73-79, 2004

[24] R. Klenk, Characterisation and Modelling of Chalcopyrite Solar Cells, *Thin Solid Films*, Vol.387, pp.135-140, 2001

[25] A.S. Gudovskikh, N.A. Kaluzhniy, V.M. Lantratov, S.A. Mintairov, M.Z. Shvarts, V.M. Andreev, Numerical Modelling of GaInP Solar Cells with AlInP and AlGaAs Windows, *Thin Solid Films*, Vol.516, pp.6739-6743, 2008

[26] N.H. Rafat, A.M. Haleem, S.E.-D. Habib, Numerical Simulation of the Limiting Efficiency of the Graded Bandgap Solar Cell, *Renewable Energy*, Vol.32, pp.21-34, 2007

[27] N. Amin, K. Sopian, M. Konagai, Numerical Modelling of CdS/CdTe and CdS/CdTe/ZnTe Solar Cells as a Function of CdTe Thickness, *Solar Energy Materials and Solar Cells*, Vol.91, pp.1202-1208, 2007

[28] A. Cuevas, A. Luque, J. Eguren and J. Del Alamo, High Efficiency Bifacial Back Surface Field Solar Cells, *Solar Cells*, Vol.3, pp.337-340, 1981

[29] J. Nijs, J. Van Meervergen, F.D'Hoore, R. Mertens and R. Van Overstraeten, High Efficiency p^+-n-n^+ Back Surface Field Silicon Solar Cells with Very Large Short-circuit Current Densities, *Solar Cells*, Vol.7, pp.331-338, 1982

[30] S.N. Singh, G.C. Jain, Effect of The Back-surface Field on The Open-circuit Voltages of p^+-n-n^+ and n^+-p-p^+ Silicon Solar Cells, *Solar Cells*, Vol.5, pp.143-172, 1982

[31] N.H. Rafat, A.M. Abdel Haleem and S.E.-D. Habib, Numerical Simulation of the Limiting Efficiency of the Graded Band gap Solar Cell, *Renewable Energy*, Vol. 32, pp.21-34, 2007

[32] A.M. Acevedo, Variable Band-gap Semiconductors as the Basis of New Solar Cells, *Solar Energy*, Vol.83, pp.1466-1471, 2009

[33] J. Robertson and B. Falabretti, Band Offsets of High K Gate Oxides on High Mobility Semiconductors, *Materials Science and Engineering: B*, Vol.135, pp.267-271, 2006

[34] D.K. Zhang, Y.C. Liu, Y.L. Liu and H. Yang, The Electrical Properties and the Interfaces of Cu_2O/ZnO/ITO p-i-n Heterojunction, *Condensed Matter*, Vol.351, pp.178-183, 2004

[35] Y.L. Liu, Y.C. Liu, H. Yang, W.B. Wang, J.G. Ma, J.Y. Zhang, Y.M. Lu, D.Z. Shen and X.W. Fan, The Optical Properties of ZnO Films Grown on Porous Si Templates, *Journal of Physics D: Applied Physics*, Vol.36, pp.2705, 2003

[36] Y. Li, F. Piret, T. Leonard and B. Su, Rutile TiO_2 Inverse Opal with Photonic Bandgap in the UV-visible Range, *Journal of Colloid and Interface Science*, Vol.348, pp.43-48, 2010

[37] V.K. Gupta, R. Jain, A. Mittal, M. Mathur and S. Sikarwar, Photochemical Degradation of the Hazardous Dye Safranin-T using TiO_2 Catalyst, *Journal of Colloid and Interface Science*, Vol.309, pp.464-469, 2007

[38] W. Siripala, A. Ivanovskaya, T. F. Jaramillo, S.H. Baeck, and E.W. McFarland, A Cu_2O/TiO_2 Heterojunction Hhin Film Cathode for Photoelectrocatalysis, *Solar Energy Materials & Solar Cells*, Vol.77, pp.229-237, 2003

[39] N. Balasubramanian and A. Subrahmanyam, Electrical and Optical Properties of Reactively Evaporated Indium Tin Oxide (ITO) Films Dependence on Substrate Temperature and Tin Concentration, *Journal of Physics D: Applied Physics*, Vol.22, pp.206-209, 1989

[40] T. Minami, T. Miyata and T. Yamamoto, Work Function of Transparent Conducting Multicomponent Oxide Thin Films Prepared by Magnetron Sputtering, *Surface and Coatings Technology*, Vol.108-109, pp.583-587, 1998

[41] N. Serin, T. Serin, S. Horzum and Y. Celik, Annealing Effects on the Properties of Copper Oxide Thin Films Prepared by Chemical Deposition, *Semiconductor Science and Technology*, Vol.20, pp.398-401, 2005

[42] F.P. Koffyberg and F.A. Benko, A Photoelectrochemical Determination of the Position of the Conduction and Valence Band Edges of p-type CuO, *Journal of Applied Physics*, Vol.53, pp.1173-1177, 1982

[43] S.Y. Sung, S.Y. Kim, K.M. Jo, J.H. Lee, J.J. Kim, S.G. Kim, K.H. Chai, S.J. Pearton, D.P. Norton and Y.W. Heo, Fabrication of p-channel Thin-film Transistors using CuO Active Layers Deposited at Low Temperature, *Applied Physics Letters*, Vol.97, pp.222109, 2010

[44] P.M. Jones, J.A. May, J.B. Reitz and E.I. Solomon, Electron Spectroscopic Studies of CH_3OH Chemisorption on Cu_2O and ZnO Single-Crystal Surfaces: Methoxide Bonding and Reactivity Related to Methanol Synthesis, *Journal of American Chemical Society*, Vol.120, pp.1506-1516, 1998

[45] W. B. Ingler Jr and S.U.M. Khan, Photoresponse of Spray Pyrolytically Synthesized Magnesium-doped Iron(III) Oxide (p-Fe_2O_3) Thin Films under Solar Simulated Light Illumination, *Thin Solid Film*, Vol.461, pp.301-308, 2004

[46] K. Kasem, Photoelectrochemical Studies on Aqueous Suspensions of 3-Dodecyl 2-5 Di-Thionyl Pyrrole/Metal Oxied Photoactive Interfaces, *Surface and Interface Analysis*, DOI:10.1002/sia.3747, 2011